PARTICLE LOSS: AN INITIAL INVESTIGATION INTO SIZE EFFECTS AND STRESS-DILATANCY

McDougall[1], J.R., Kelly[2], D. & Barreto[1], D.

[1] School of Engineering and Built Environment, Edinburgh Napier University, UK.
[2] Independent Consultant, Edinburgh, UK

Corresponding Author:

Dr J.R. McDougall
School of Engineering and the Built Environment,
Edinburgh Napier University
10 Colinton Rd
Edinburgh, EH10 5DT

j.mcdougall@napier.ac.uk
0131 455 2533

Words: 4510 (excl abstract & references & fig captions)
5269
Figures: 15
Tables: 5

PARTICLE LOSS: A STRESS-DILATANCY APPROACH TO SIZE EFFECTS

ABSTRACT

Drained triaxial tests have been performed to explore the effect of particle loss on shearing behaviour and critical states in granular mixtures. The mixtures comprise Leighton Buzzard sand (d_{50} = 0.8 mm), to which was added 15% by mass of salt particles of different nominal sizes: 0.063 mm, 0.25 mm and 0.5 mm. Shearing behaviours before and after particle loss (by dissolution) were compared. A good fit is observed between the test data and a stress-dilatancy relationship for the post-dissolution tests, highlighting the ability of the stress-dilatancy analysis as a means to interpret the effects of particle loss on shearing. It was noted that critical state strength parameter M is determined by the post-dissolution grading regardless of size of removed particle. However, the duration of contractant volumetric strain increased with the larger removed particles (0.25 mm & 0.5 mm) even when initial specific volumes were virtually identical. It is suggested that a loose volumetric state is reached if the sand particle network is initially disrupted by the amount and/or size of salt particles, which following dissolution results in structural or fabric phenomena that are not reflected in scalar volumetric measures such as specific volume.

Keywords: Soluble soils, particle loss, laboratory testing, triaxial testing, stress-dilatancy

INTRODUCTION

There is widespread recognition that particle loss in granular materials leads to significant changes in soil structure with consequences for volume and shear strength (Xiao and Shwiyhat, 2012). Particle loss may be due to internal erosion in dams, biodegradation in landfills or dissolution. Regardless of the mechanism of particle loss, the consequences are geotechnical and commonly dependent on the amount, size and gradation of lost particles. Much of this work has hitherto focussed on the amount of fine material removed. This paper is an early exploration of the effect of lost particle size.

Ke and Takahashi (2012) made a series of internal erosion tests in which up to 25% by mass of fines were removed. Samples were then subject to miniature cone penetration tests. They noted a reduction in soil strength. Scholtes et al (2010), using both DEM and analytical models, simulated losses of 5% of the smaller particles from a well-graded granular assembly. They concluded that particle removal leads to an increase in porosity and reduction in 'internal angle of friction' of about 4° between initial intact and degraded states, where the latter refers to the residual value. Andrianatrehina et al (2016), from a series of triaxial tests on gap-graded gravel sand mixtures, observed that removal of (up to 30%) fines produced lower undrained peak strength. Their tests reveal a transition from dilatant to contractant shearing behaviour; intact specimens (with 30% fines) were dominated by dilatant behaviour while samples with the smallest amount of fines (5%) were characterised by a contractant response. Scholtes et al (2010) also commented on degraded soils behaving like a loose material with significant contraction and a gradual rise in stress ratio.

In contrast, Ke & Takahashi (2014) performed triaxial tests in which between 15% and 35% of fines content were removed. Mainly ductile deviator stress-axial strain responses were reported, which at small strains (up to 1%) revealed higher deviator stresses in the samples from which particles had been flushed, although later work by the same authors (Ke and Takahashi, 2015) suggested that

fines removal is likely to produce a general reduction in soil strength. Ouyang and Takahashi (2016) observed that after internal erosion, soils became less contractant and revealed an increase in shearing resistance. They postulated that increases in soil strength following erosion are due to 'jamming' caused by the re-deposition of migrating fines around coarse grain contact points. In the case of erosion, only particles small enough to move through the coarse void network can be lost so particle loss is synonymous with fines removal. No such limitation exists in the case of dissolution, where larger particles dissolve into the pore liquid and are lost to the solid phase.

Particle loss by dissolution and its effect on soil properties have been explored by Fam et al (2002), Shin & Santamarina (2009) and Truong et al (2010), all of whom addressed the effect of loss of different amounts of a single size particle. McDougall et al (2013) investigated the effect of both amount and particle size under oedometric conditions. In all cases, particle loss is accompanied by an increase in specific volume. Tran et al (2012) studied the shearing resistance of post-dissolution salt-sand mixtures in the direct shear box and using DEM. They noted a more ductile response of the post-dissolution material on shearing. Cha & Santamarina (2013) drew similar conclusions from 3D DEM simulations. They also noted increases in specific volume on dissolution with post-dissolution shearing evolving towards a common critical state. Muir-Wood & Maeda (2010) using DEM, showed strength behaviour to be relatively insensitive to changes in grading. In contrast, the critical state line in mean effective stress specific volume space increased with narrower grading distributions, in other words, a well-graded sand shows a higher critical specific volume for any given mean stress.

This paper describes an experimental investigation into the triaxial shearing of granular mixtures from which an initial 15% of soluble particle content of specified particle size has been removed. Shearing behaviour both before (intact) and after dissolution over a range of soluble particle sizes

are compared. The results are interpreted in terms of both their stress-strain and stress-dilatancy behaviour.

Stress-dilatancy

The stress-strain behaviour and critical states of loose and structured sands have been investigated in the context of stress-dilatancy by a number of workers, in particular Been & Jefferies (2004), Consoli et al (2012) and Bhandari & Powrie (2013)

Been & Jefferies (2004) reported a series of drained triaxial tests on dense and loose Erksak sand. Dense sands rise steeply (see Fig.1) at the start of shearing to a stress-dilatancy relationship, in this case a Cam Clay relationship,

$$D = M - \eta \qquad (1)$$

where D is the dilation rate, η is the ratio of deviator stress to mean stress and *M* is the value of η at critical state, i.e. the critical state strength parameter. This linear relationship (with M = 1.05) is followed until a reversal occurs, at which point a peak stress ratio and maximum rate of dilation are defined. The sample then moves back towards the critical state. In contrast, loose samples climb shallowly to the right, confirming an early pronounced contraction, to reach their stress-dilatancy line (SDL) at stress ratios of about 0.4. The stress-dilatancy path then follows a Cam clay relationship with M = 1.26, rising gradually under contractant conditions to a critical state.

Bhandari & Powrie (2013) performed triaxial tests on interlocked Reigate sand. At low cell pressures, see 12.5 kPa in Fig. 2, stress ratios for both interlocked and reconstituted samples rise initially steeply to the SDL, indicating a dense shearing behaviour. In the case of the interlocked samples, stress ratios rise well above the SDL. At higher cell pressures (100 kPa), the initial stress path resembles that observed by Been & Jefferies' loose sands, i.e. a more contractant path rising at first shallowly to the SDL. Two SDLs are shown in Fig.2: the first with M = 1.22, which fits well the

linear path followed by both reconstituted samples while dilating. The other with M = 1.5 marks the critical state to which both interlocked samples and the low pressure reconstituted sample appear to tend.

Consoli et al (2012) also investigated the stress-dilatancy behaviour of cemented sands at confining pressures of 20 to 400 kPa. Where cell pressures are low (tests T-01 & T-04 in Fig. 3), a steep climb to high stress ratios like that described by Been & Jeffries for the Erksak dense sands and Bhandari & Powrie 12 kPa confining pressure tests can be seen. In contrast, high cell pressures reveal a loose soil response (tests T-03 & T-06 in Fig. 3), where samples contract with increasing stress ratio until turning to follow a SDL to the critical state. A common SDL is not so well defined here, probably because changes in particle shape and grading characteristics associated with the breakage of cement bonds, result in different critical states.

TEST PROGRAMME

Twelve drained triaxial tests have been performed: 2 sand-only and 10 salt-sand mixtures. Of the 10 salt-sand mixtures, 3 were sheared intact (undissolved), the remaining 7 were inundated to remove by dissolution the salt particles before shearing. The test results are presented in two groups; the first to indicate something of the shearing characteristics of intact salt-sand (ISS) mixtures, comprising salt particles of three different sizes. These results are offered as indicative behaviours only, for reasons highlighted later. Secondly, all 7 DSS mixtures are compared to evaluate the effect of removed particle size. The two sand-only tests are included in both groups. The DSS mixtures were tested at a range of confining pressures; however, previous oedometer testing (McDougall et al, 2013) showed volume changes during dissolution to be insensitive to the level of confining pressure used here.

The sand was Leighton Buzzard, a sub-rounded quartz sand with d_{50} = 0.85 mm, coefficient of uniformity = 1.4 and particle specific gravity = 2.65. Each of the salt-sand mixtures contained 15% by mass of salt; the salt fraction consisted of particles of one of the following nominal specific sizes: 0.063 mm, 0.25 mm & 0.5 mm. Figure 4 shows the particle size distributions for each of the salt-sand mixtures and Table 1 summarises the test programme. The salt was sodium chloride, which after crushing has a more angular form. Particle specific gravity = 2.165. Figure 5 shows the sizes and shapes of sand and two of the salt particle fractions. For the sand-only and ISS mixtures triaxial shearing comprised the usual stages: isotropic compression and shearing; the DSS tests comprised three stages: isotropic compression, dissolution and then shearing.

Equipment: general constraints & triaxial cell modifications

All sand-salt mixtures were dry during the isotropic compression stage. Dissolved samples were then flooded and pore water circulated to dissolve salt particles. Because the sample is dry during compression and pore fluid circulated without pressure control during shearing, changes in sample volume had to be deduced from changes in cell volume, the details of which are given below.

Salt saturation of the pore water and hence inhibition of the dissolution process was avoided by a recirculation system. The system comprised a 5 L reservoir, which provides sufficient water volume to dissolve all salt, and peristaltic pump to circulate solution upwards through the sample and back to the reservoir. The reservoir was fitted with stirrer and conductivity probe to monitor dissolution. In previous work we have confirmed complete dissolution when a steady conductivity probe reading is achieved, usually within 30 minutes, then by drying and weighing of the remnant fraction (McDougall et al., 2013). Water level in the reservoir was at just above the top of the sample. Figure 6 shows the modified cell and recirculation apparatus.

Sample preparation

The dry salt-sand particles were mixed and riffled into eight parts. Each part was deposited in the sample former on the triaxial pedestal using a funnel to minimise drop height and avoid segregation. Each part was compacted by placing a cylindrical steel weight into the sample former then vibrated using a small vibrating engraving tool for 10 seconds.

Sample volume changes.

Sample volume changes were determined from cell volume changes recorded by a GDS ELDPC volume/pressure controller after consideration of ram displacement, cell compliance, membrane penetration and dissolution.

Although the GDS controller has a quoted volumetric accuracy of 0.4%, its performance was checked by comparison of reported volume changes with known volume changes based on ram displacement. An average measured volume change of 0.301 ml/mm ram displacement was observed compared with a calculated volume change of 0.284 ml/mm. The discrepancy of 0.017 ml/mm is equivalent to a 6% over-reporting of the true cell volume change. Total volume changes of about 15 ml were recorded during dissolution in the 0.5 mm salt particle size mixtures. Table 2 shows the phase volumes for a typical test sample before and after dissolution where the measured total volume changes are 15 ml and 15.9 ml, the latter representing a 6% overestimate in the GDS reading. Given the size of the triaxial sample, a 6% error in the GDS reporting of volume transfers, translates into post-dissolution specific volumes of 1.742 and 1.733, in other words a negligible impact on specific volume calculations.

A volumetric adjustment based on ram diameter was made for ram displacement. Cell compliance was checked (Kelly, 2014) and considered not to be significant during cell pressurisation compared with the magnitude of volume changes occurring due to dissolution, which ranged between 2 ml and 16 ml for the 0.063 & 0.5 mm salt particles respectively. Nor was absorption of moisture by the

acrylic cell regarded as a problem over the duration of the shearing stage (about 1 hr). An adjustment for membrane penetration was made using the method described by Nicholson et al (1993).

Initial conditions & dissolution

Figure 7 shows the pre- and post-dissolution specific volumes as data points joined by a vertical line. Since all mixtures increased in specific volume with dissolution, the lower data point depicts the pre-dissolution specific volume and the upper data point that of the post-dissolution condition. Samples comprising 0.5 mm and 0.25 mm salt particles have a similar initial specific volume to that of the sand-only samples (see also Table 3). In the case of the 0.063 mm salt particles, specific volumes fall below the minimum of the sand alone; these particles are able to 'nestle' between larger sand grains. Larger salt particles cannot nestle and are part of the inert sand particle network. In all cases, dissolution causes an increase in specific volume[1]. The 0.5 mm and 0.25 mm salt particle reveal increases in specific volume of ≈0.20 and are brought to a loose state with specific volumes of ≈1.78. The 0.063 mm particle samples show a larger increase in specific volume, ≈0.28, but only reach specific volumes of ≈1.69. The implication of this is that the 0.063 mm particles are removed with less sand particle rearrangement, i.e. lower overall volume change, than is the case with the larger salt particles.

RESULTS

Dissolved salt-sand (DSS) vs. intact salt-sand (ISS) mixtures – stress-strain & stress dilatancy

Figure 8a shows the stress ratio-axial strain behaviour of three ISS tests (#22, 23, 25) and one sand-only test (#3). Salt particle sizes are 0.063, 0.25, and 0.5 mm. Samples were sheared at a confining stress of 168 kPa. The presence of 0.063 mm particles (#25), produces a lower initial specific volume

[1] *In a dissolving soil, changes in specific volume, $\nu = (V_s + V_v)/V_s$, can be caused by either void or solid volumes. A loss of solid particles or solid phase volume, which triggers an equivalent increase in void volume, produces a marked (maximum) increase in specific volume with no overall volume change (or settlement).*

(ν = 1.44) than the sand-only sample (ν = 1.54), which in turn increases the peak stress ratio and delays its full mobilisation from an axial strain of ≈ 3% in the sand-only test to ≈ 7% in the mixture. The presence of 0.25 mm particles (#23, ν = 1.54) leads to a peak of approximately the same magnitude as the sand-only test, with full mobilisation also ≈ 7%. With the addition of 0.5 mm particles (#22, ν = 1.56), a slightly lower peak is obtained. Hence, the presence of fine particles, which can nestle within the sand particle matrix and reduce the specific volume, increases peak strength compared with the sand-only tests. The addition of larger particles, which has little impact on either specific volume or particle grading, reveals peak stress ratios similar to the sand-only test, as may be expected, but at greater axial strains.

Figure 8b shows tests 9, 11 and 4, which are the dissolved counterparts of tests 22, 23 & 25, also confined at 168 kPa. Post-dissolution specific volumes are 1.67, 1.75 and 1.77 respectively (see Table 3). It is evident that dissolution brings about a marked reduction in strength and more ductile shearing response, which appears directly related to size of the removed particles and consistent with the associated post-dissolution specific volumes. Bear in mind that that the ISS and DSS mixtures were sheared in dry and wet conditions respectively. However, Lambe and Whitman (1969) and Senetakis et al (2013), the latter working with Leighton Buzzard sand, observed that particles immersed in water showed very similar friction properties to those in a dry state. Of course the ISS mixtures are complicated by the presence of a salt fraction but we contend that the dry tests at least provide a credible indication of the wet intact salt-sand behaviour.

A more probing comparison of the shearing behaviour of these tests can be obtained from a stress-dilatancy analysis, as shown in Fig. 9. Using a Nova (1982) type stress-dilatancy relationship, i.e.

$$D = \left(\frac{M-\eta}{1-N}\right) \tag{2}$$

where N is a fitting parameter (here = 0.2), the three ISS tests and one sand-only test (#3) point to a quantifiable influence of grading on critical state strength parameter M. Compared to the sand-only test, where M = 1.24, the addition of salt particles causes an increase in M.

Figure 10 shows M to vary directly with the diameter (d_{50}) ratio of inert sand to added salt. In other words, increases in M are greatest where the added salt particles, at this percentage amount, are small. Figure 10 also shows data from Papadopoulou and Tika (2008) for (i) a rounded quartz sand only and (ii) sand with 15% (by mass) fines addition (diameter ratio = 15), from which a rate of increase of M with diameter ratio of added particles, similar to that observed in this study, can be seen. It should be borne in mind that the increases in M with diameter ratio shown in Fig. 10 can be attributed to two factors: salt/fines addition and particle shape in the ISS mixtures.

The findings relating to M should be treated cautiously because of the impact of crushing. Whilst crushing is unlikely to affect sand particles, there is a question over the crushing of salt particles. Crushing is most likely to affect the larger salt particle sizes (0.25 & 0.5 mm) that are present in the ISS tests and participating in strong force chain networks. The effect of crushing will be to increase the amount of fine salt particles. In DSS tests salt particles are only present during the compression stage and salt crushing at these confining stresses under oedometric loading was not found to be a problem (McDougall et al, 2013).

The DSS samples (#9, 11 & 4) all reveal a value of M = 1.24 with N = 0.2 (Fig. 9 & Table 3) underlining the conclusion that the shear strength characteristics of a post-removal sand are controlled by the remnant grading.

Dissolved salt-sand (DSS) mixtures by particle size: stress ratio-axial strain

In this section, four other DSS tests (#7, 8, 10 & 12), at confining stresses of 42 and 84 kPa (see Table 1) and one other sand-only test (#1) are considered along with the three DSS tests from the previous section (#9, 11 & 4, confined at 168 kPa).

Figure 11 shows the stress ratio-axial strain results for all nine tests. The brittleness of the sand-only tests is replaced by a more ductile response in the tests from which particles have been removed. Moreover, the larger the size of the removed salt particle, the more ductile is the response. An explanation for such an effect may be sought in the initial specific volumes. For example, Fig. 7 and Table 4 show that sand-only samples have initial specific volumes 1.53 and 1.54, the post-dissolution specific volume of 0.063 mm mixtures is ≈1.68, while the 0.25 mm and 0.5 mm mixtures = 1.75 and 1.76 respectively. While the post-dissolution specific volumes of the 0.25 mm and 0.5 mm mixtures are nearly identical, the position of the stress-strain curves reflect the pattern of increasing ductility that would be revealed by mixtures with higher specific volumes (Fig. 11). Although it is not possible to advance a conclusive explanation on the basis of the monitoring undertaken here, it will be the case that the larger salt particles are too big to nestle within the sand skeleton and are likely to be key elements or lateral supporters of strong force chains. Dissolution of large salt particles allows for the agglomeration of remnant sand particles in the loosest possible state. That both 0.25 mm and 0.5 mm mixtures show more or less the same post-dissolution specific volume is plausible, suggesting that a kind of loosest possible volumetric state of the sand is reached if the pre-dissolution particle arrangement is 'held up' by a combination of amount and/or size of salt particles. In this case, 15% of 0.25 mm particles is sufficient to bring about this near maximum specific volume state.

Volumetric strain – dissolved-salt-sand mixtures

Volumetric strain behaviour is shown in Fig. 12. Angles of dilation are greatest at axial strains of 1% to 2% in the sand-only samples. The 0.063 mm mixtures also show a dilatant response but not

before a prolonged contractant phase, to ≈ 2.5% axial strain. Similarly, the 0.25 mm mixtures contract up to ≈ 4% axial strain. Interestingly, the 0.5 mm mixtures are predominantly contractant up to ≈10% axial strains, even though their initial specific volumes were the same as those observed for the 0.25 mm mixtures.

The volumetric strain data shows a consistent response to the size of lost particles, i.e. dilatant switching to contractant, at least up to 0.25 mm mixtures, yet initial specific volumes are not unambiguously consistent in this regard. As noted in the previous section, the ongoing increase in ductility, here manifest as a more pronounced contractancy are found in the two larger salt particle mixtures, which have nearly identical initial specific volumes.

Dissolved salt-sand (DSS) mixtures by particle size: stress dilatancy

Figure 13 shows the stress-dilatancy responses of the two sand-only and all 7 DSS tests. A single Cam clay stress-dilatancy relationship, Eq(1), with M = 1.24 is also shown. Of interest here are the paths to the SDL taken by the nine tests. The sand-only samples (#1 & 3) being strongly dilatant rise initially vertically to the stress-dilatancy relationship whereas the DSS tests climb shallowly to the right, reflecting the contractant behaviour observed during mobilisation of shearing resistance. A clearer quantitative interpretation of the stress-dilatancy response is obtained if the test mixtures are considered separately, i.e. as sand-only samples and then by salt particle size.

The sand-only tests (#1 & 3) are shown in Fig. 14a. The initial mobilisation of shearing resistance up to and above the stress dilatancy relationship line is evident. Stress ratio paths then turn to the left. Maximum dilation (D_{peak}) and peak stress ratio (η_{peak}) are reached, at which point the paths reverse, following the stress-dilatancy relationship towards the critical state, but not reaching it because of the constraints of the triaxial test. The Cam clay stress-dilatancy relationship, Eqn (1), with M = 1.24 is shown along with the data for the two sand tests. Table 5 shows the maximum/peak dilation rates

and stress ratios (averaged for each particle size mixture), and critical state strength parameters for all tests.

Figure 14b shows the stress-dilatancy behaviour for the 0.063 mm DSS mixture tests (# 9, 10). The stress ratio paths climb shallowly to the right. Initially contractant behaviour gives way to dilatant shearing. Peak stress ratios are reached, which at 1.44, are much lower than those observed in the sand-only tests, where η_{peak} = 1.78 (Fig 14a & Table 5). Reversal follows as the samples move back towards but, like the sand-only tests, do not reach a critical state. The stress-dilatancy data fit well the Cam-clay function, with M = 1.24.

Figure 14c shows stress-dilatancy of the 0.25 mm DSS tests. A similar pattern of behaviour to that observed in the 0.063 mm DSS tests is evident, although the reach of the stress ratio path into dilatant territory is shorter to a dilation rate of – 0.13. (#11 & 12).

Figure 14d shows stress-dilatancy for the 0.5 mm DSS tests. All stress dilatancy paths rise towards and terminate at or close to the critical state. There is little evidence of dilatant behaviour, maximum dilation rate = – 0.01 (#4, 7 & 8). The Cam-clay stress dilatancy relationship with M = 1.24 is again shown.

Discussion

A common stress-dilatancy relationship can be fitted to the DSS test data to provide a framework in which a more probing interpretation of the shear stress-strain and volumetric strain responses to particle loss can be made. Not only are critical states elucidated, the dilatant response of the sand-only tests and an increasingly contractant behaviour with size of removed particle in the DSS tests is distinguished. Referring to Fig. 15, sand-only tests follow path ACDE, whilst DSS tests follow path ABE. Interestingly, the 7 DSS tests show little influence of dissolved particle size on their approach

to the SDL. However, they distinguish themselves in a consistent manner by the extent to which their paths enter into the dilatant part of the diagram. Small salt particles (at this percentage), despite an initially pronounced contractant response, move along the SDL to become dilatant before moving back down the line towards the critical state. The maximum dilation rate found in the 0.063 mm DSS tests is marked in Fig. 15. While the 0.25 mm and 0.5 mm DSS tests can be distinguished by their travel into the dilatant part of the diagram, they have virtually identical specific volumes. The 0.25 mm DSS tests reveal some dilatancy, albeit after a considerable period of contractancy, up to axial strains of 10%, whilst the 0.5 mm DSS tests are predominantly contractant throughout. The stress paths revealed are consistent with behaviour outlined previously and as described by Been & Jefferies (2004), Bhandari & Powrie (2013) and Consoli et al (2012) for loose and dense sands.

SUMMARY & CONCLUSIONS

The test data and stress-dilatancy analysis presented here are relevant to and build upon the body of research on internal stability and the mechanical consequences of particle loss. Whilst internal stability is well characterised by analysis of the loss of fines, the data here cover a range of removed particle sizes, up to about the same size as the well-graded remnant sand host. They show that post-removal mechanical behaviour is elucidated by both stress-strain and stress-dilatancy approaches. In particular, both approaches highlight the emergence of more ductile post-removal behaviour.

Stress-dilatancy confirms that a common critical state is identified for the post-removal mixtures over the range of salt particle sizes and that the common end state is approached by increasingly pronounced periods of contractancy that eventually give way to dilatant behaviour. Interestingly, a consistent increase in contractancy (or ductility) associated with increasing size of particle removed, appears not to be revealed by the initial (post-dissolution) specific volumes. Specifically, 0.25 mm and 0.5 mm DSS mixtures were observed to have virtually identical initial specific volumes (1.75 and

1.76 respectively) yet they were distinguished by the extent to which they travelled into the dilatant side of the stress-dilatancy diagram. In the stress strain plots, the 0.25 mm DSS tests showed a small amount of dilatancy after about 10% axial strain whereas the 0.5 mm DSS tests were almost entirely contractant. Thus it may be suggested that there are structural phenomena that are not captured by a scalar volumetric measure such as specific volume or density. These structural phenomena or fabric effects, may well comprise sand skeleton force chain networks and lateral support that are influenced by large particle loss in a way that is not reflected in a scalar measure such as specific volume. The impact of large particle removal and mechanical consequences is outside the scope of the current work but is the subject of ongoing investigation.

REFERENCES

Andrianatrehina, N.L, Souli, H., Rech, J.,Fry, J-J., Fleureau, J-M and Taibi, S.l (2016) Influence of percentage of sand on the behaviour of gap-graded cohesionless soils. *Comptes Rendus Mecanique* **344**, 539-546.

Been, K. and Jefferies, M. (2004). Stress–dilatancy in very loose sand. *Canadian Geotechnical Journal* 41, 972-989. doi: 10.1139/T04-038

Bhandari, A. and Powrie, W. (2013). Strength and deformation characteristics of a locked sand at low effective stresses. *Granular Matter* **15**, 543-556. doi:10.1007/s10035-013-0426-8

Cha, M. and Santamarina, J.C. (2013). Dissolution of randomly distributed soluble grains; post-dissolution k0-loading and shear. *Géotechnique* **64**, No 10, 828-836

Consoli, N.C., Cruz, R.C., Viana da Fonseca, A. and Coop, M.C. (2012). Influence of Cement-Voids Ratio on Stress-Dilatancy Behavior of Artificially Cemented Sand. *J. Geotechnical and Geoenvironmental Eng*. **138,** No 1, 100-110. doi: 10.1061/(ASCE)GT.1943-5606.0000565.

Fam M.A., Cascante, G. and Dusseault, M.B. (2002) Large and small strain properties of sands subjected to local void increase. *J. of Geotechnical and Geoenvironmental Eng*. **128**, No 12, 1018-1025

Ke, L. and Takahashi, A. (2012) Strength reduction of cohesionless soil due to internal erosion induced by one-dimensional upward seepage flow. *Soils and Foundations*, **52(4)**, 698-711.

Ke, L. and Takahashi, A. (2014) Experimental investigations on suffusion characteristics and its mechanical consequences on saturated cohesionless soil. *Soils and Foundations* **54**, 713-730.

Ke, L. and Takahashi, A. (2015) Drained monotonic responses of suffusional cohesionless soils. *J. Geotechnical and Geoenvironmental Eng*. **141**, No 8,

Kelly, D. (2014). Effect of particle loss on soil volume, strength and stiffness. *Submitted in fulfilment of requirements of PhD*, Edinburgh Napier University.

Lambe, T.W. and Whitman, R.V. (1969) Soil mechanics. John Wiley, New York.

McDougall, J.R, Kelly, D. and Barreto, D. (2013). Particle loss and volume change on dissolution: experimental results and analysis of particle size and amount effects. *Acta Geotechnica* **8**, 619–627. doi 10.1007/s11440-013-0212-0

Muir-Wood, D. and Maeda, K. (2008). Changing grading of soil: effect on critical states. *Acta Geotechnica* 3, 3-14. doi: 10.1007/s11440-007-0041-0

Nicholson, P., Seed, R. and Anwar, H. (1993), Elimination of membrane compliance in undrained triaxial testing. ii. Mitigation by injection compensation, *Canadian Geotechnical Journal* **30**, 739–746.

Nova, R. (1982). A constitutive model under monotonic and cyclic loading. *In Soil mechanics — transient and cyclic loads. Edited by G. Pande and O.C. Zienkiewicz. John Wiley and Sons Ltd., New York. 343–373.*

Ouyang, M. and Takahashi, A. (2016) Influence of initial fines content on fabric of soils subjected to internal erosion. *Canadian Geotechnical Journal* **53**, 299-313

Papadopoulou, A. and Tika, T. (2008) The effect of fines on critical state and liquefaction resistance characteristics of non-plastic silty sands. Soils and Foundations **48**, 713-725.

Scholtes, L., Hicher, P-Y. and Sibille, L. (2010) Multiscale approaches to describe mechanical responses induced by particle removal in granular materials. *Comptes Rendus Mecanique* 338, 627-638.

Senetakis, K. Coop, M.R. and Todisco, M.C. (2013) The inter-particle coefficient of friction at the contacts of Leighton Buzzard sand quartz minerals. Soils and Foundations, **53(5)**, 746-755.

Shin, H. and Santamarina, J.C. (2009) Mineral dissolution and the evolution of k_0. *J. Geotechnical and Geoenvironmental Eng*. **135**, No 9, 1141-1147

Tran, M.K., Shin, H., Byun, Y-H. and Lee, J-S. (2011) Mineral dissolution effects on mechanical strength. Engineering Geology **125**, 26-34.

Truong, Q.H., Eom Y.H., Lee, J-S. (2010) Stiffness characteristics of soluble mixtures. *Géotechnique* **60**, No4, 293-298

Xiao, M. and Shwiyhat, N. (2012) Experimental investigation of the effects of suffusion on physical and geomechanics of sandy soils. *Geotechnical Testing Journal*, **35(6)**, 1-11.

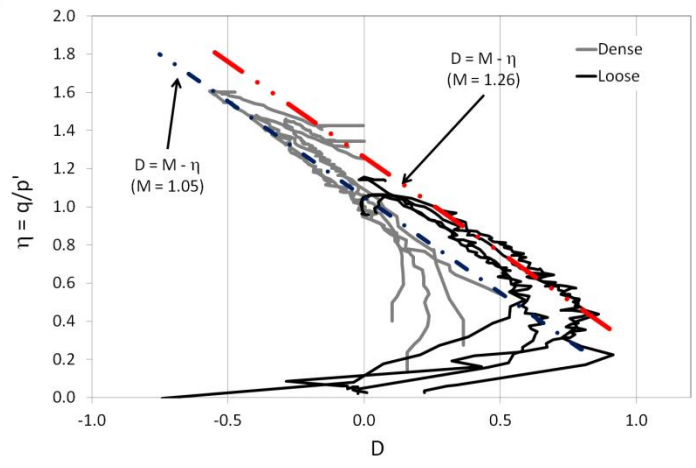

Fig. 1. Stress–dilatancy relationships measured in tests on loose and dense Erksak sands (modified from Been & Jefferies, 2004)

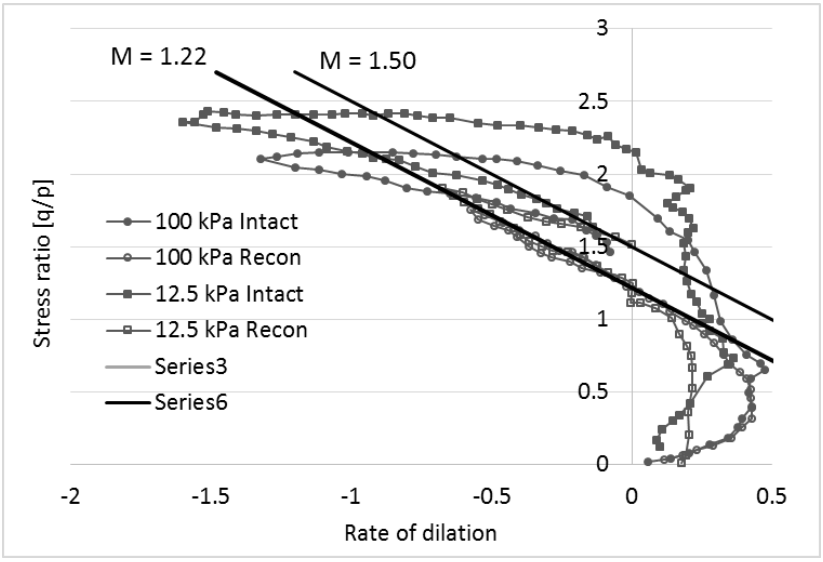

Fig.2. Stress–dilatancy in drained triaxial compression test at effective cell pressures of 12.5 kPa and 100 kPa for intact and reconstituted specimens of interlocked Reigate silver sand (modified from Bhandari & Powrie, 2013.

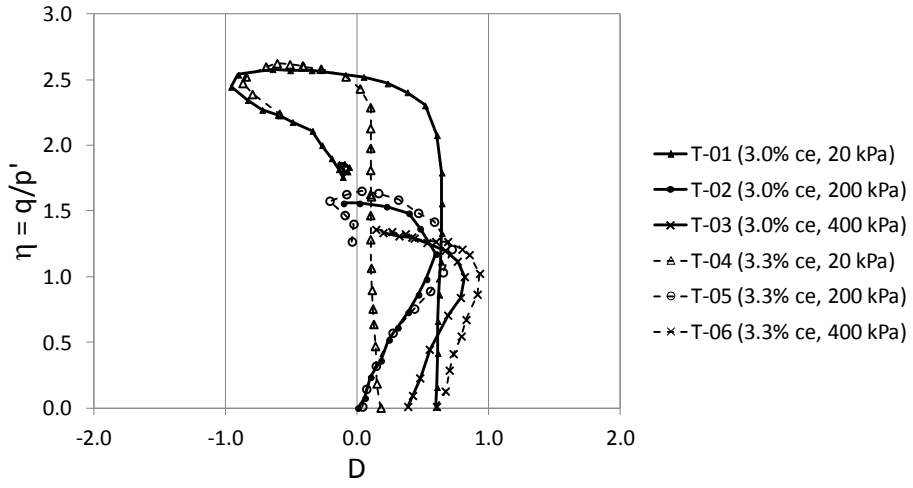

Fig. 3 Stress–dilatancy relationships for cemented soils, cement contents of 3% - 3.3% (drawn from Consoli et al, 2012)

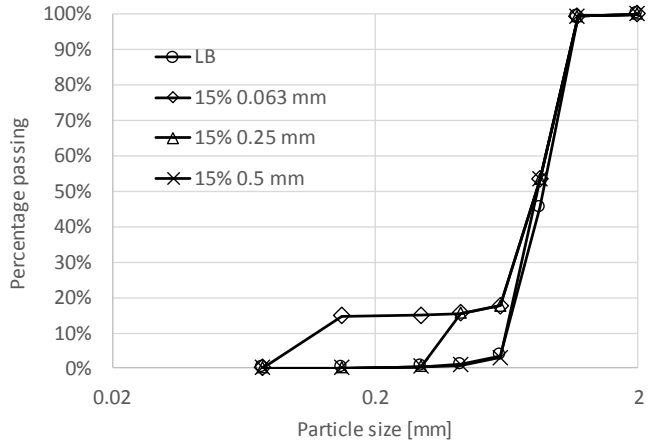

Fig. 4. Particle size distributions for Leighton Buzzard sand and the three salt-sand mixtures: 15% of 0.063 mm, 0.25 mm & 0.5 mm salt particles.

a) 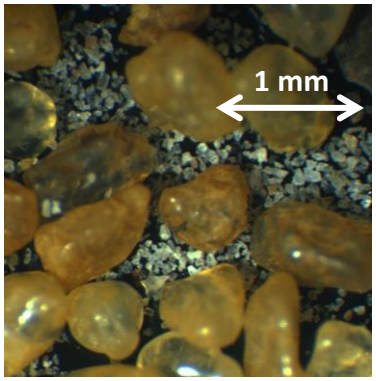

b) 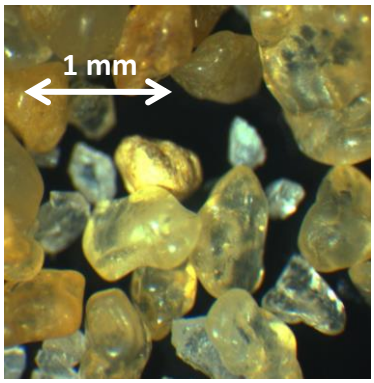

Fig. 5. Sand-salt mixes showing relative sizes and shapes: (a) Leighton Buzzard sand and 0.063 mm salt, (b) Leighton Buzzard sand and 0.25 mm salt.

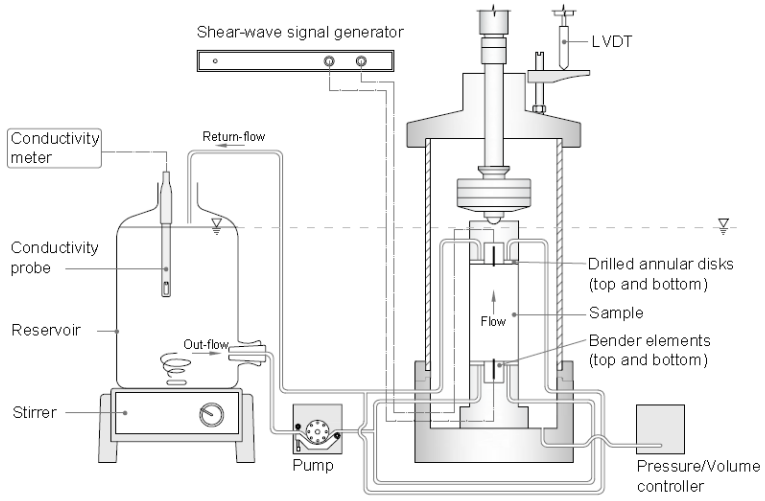

Fig. 6. Triaxial apparatus plus equipment additions and modifications required to allow salt dissolution.

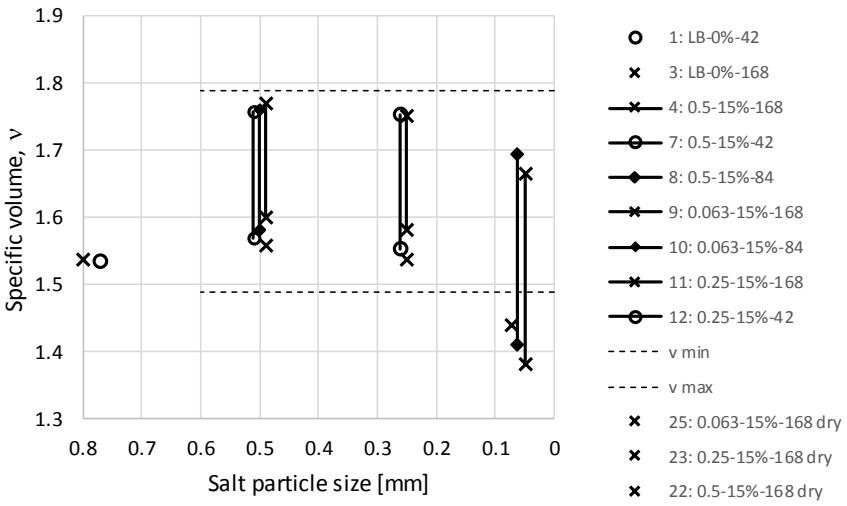

Fig. 7. Pre- and post-dissolution specific volumes by particle size and cell pressure. Legend shows test number: size of salt particle in mm – percentage mass of salt – cell pressure. Cell pressure also identified by symbols: ○= 42 kPa, ◆ = 84 kPa, x = 168 kPa. Also shown are minimum and maximum specific volumes for the sand-only samples. Single data points are sand-only tests (shown at 0.8 mm salt particle size) or dry salt-sand mixtures (shown as an unattached x symbol); data points joined by a vertical line depict the combination of pre-dissolution (lower) and post dissolution (upper) data points. In all cases dissolution led to an increase in specific volume.

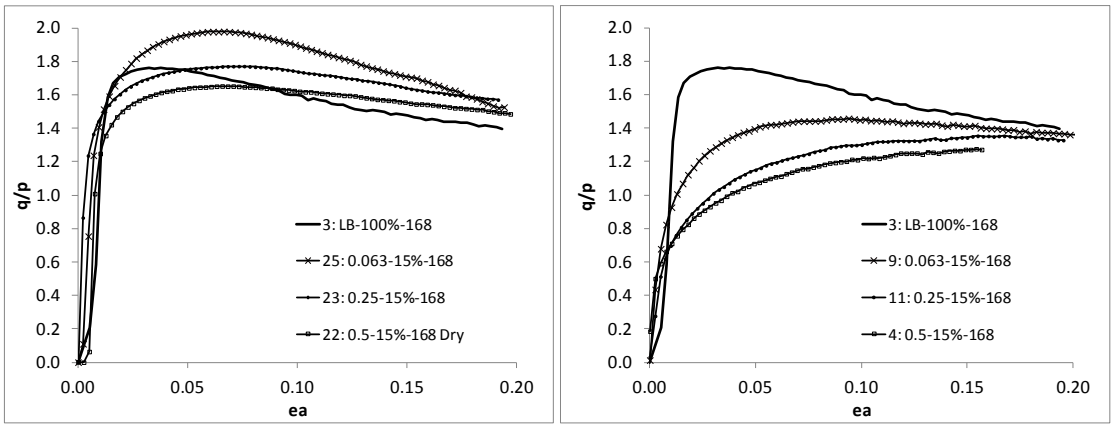

Fig. 8a. Stress ratio-axial strain curves for intact-salt sand and (b) corresponding dissolved-salt sand mixtures

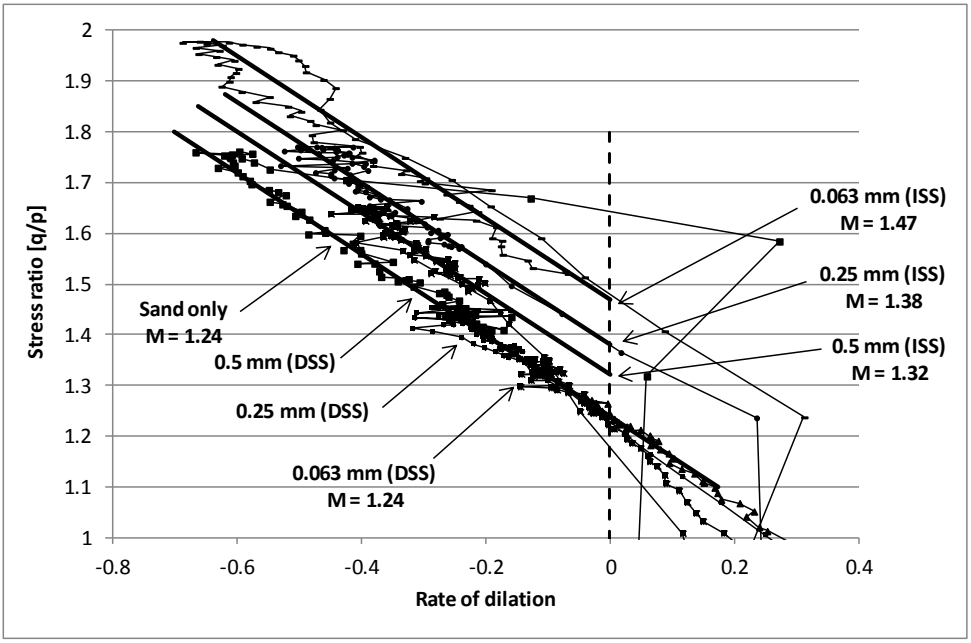

Fig. 9. Close up of stress-dilatancy for intact-salt- sand and corresponding dissolved-salt-sand mixtures together with fitted stress-dilatancy relationship lines, all of the Nova (1982) type with M values as stated and N = 0.2.

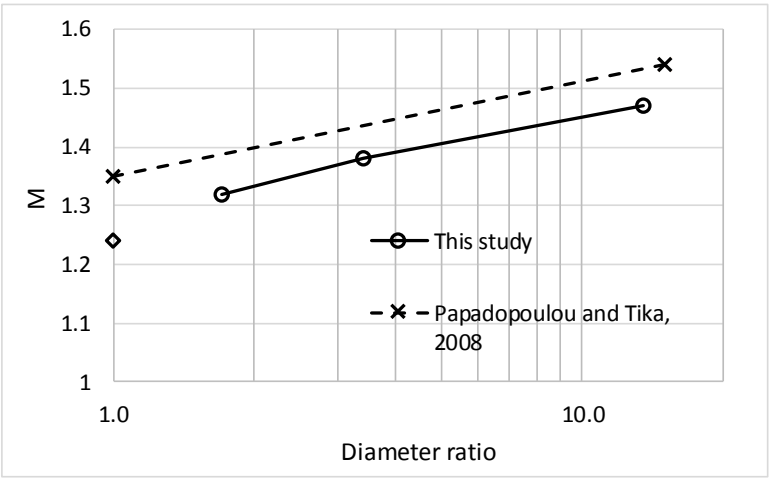

Fig. 10. Variation of critical state strength parameter M with size of added salt particles depicted by d_{50} diameter ratio (of sand to salt particles). Diameter ratio = 1.0 corresponds to the sand only test.

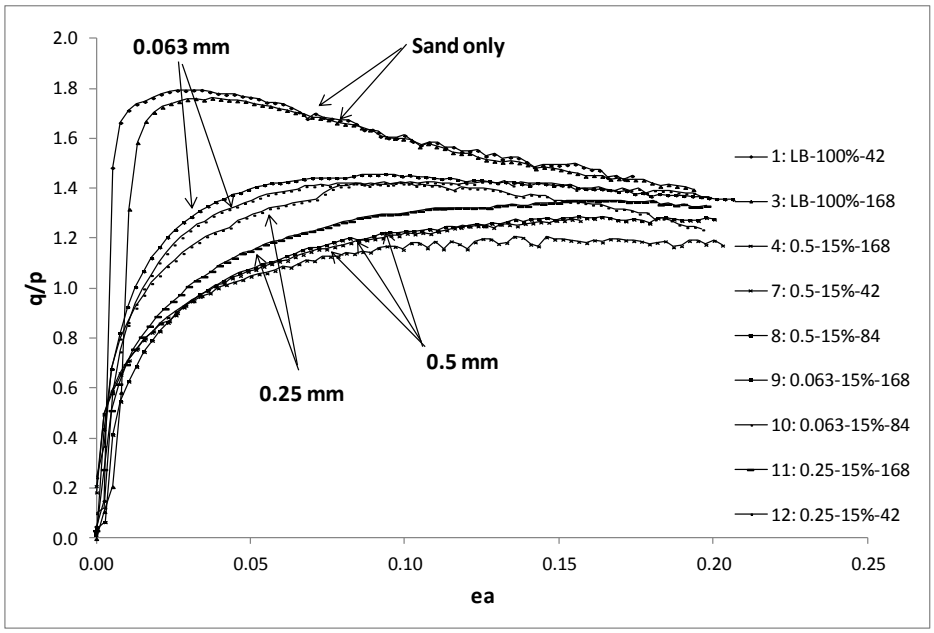

Fig. 11. Stress ratio–axial strain data for sand only (#1 & 3) and 7 DSS (#4, 7, 8, 9, 10, 11, & 12) samples.

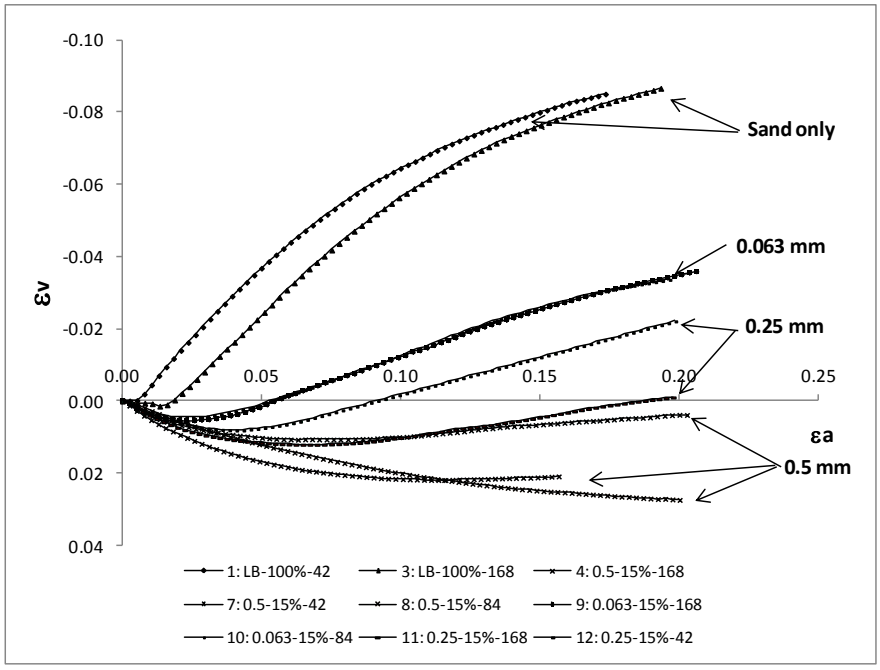

Fig. 12. Volumetric strain-axial strain data for sand only (#1 & 3) and DSS samples.

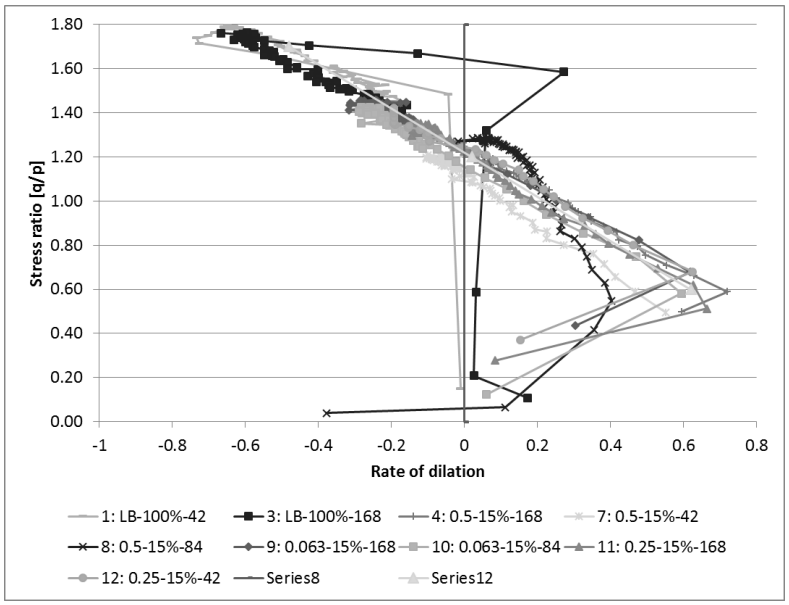

Fig. 13. Stress-dilatancy for all tests: sand-only and dissolved salt-sand mixtures.

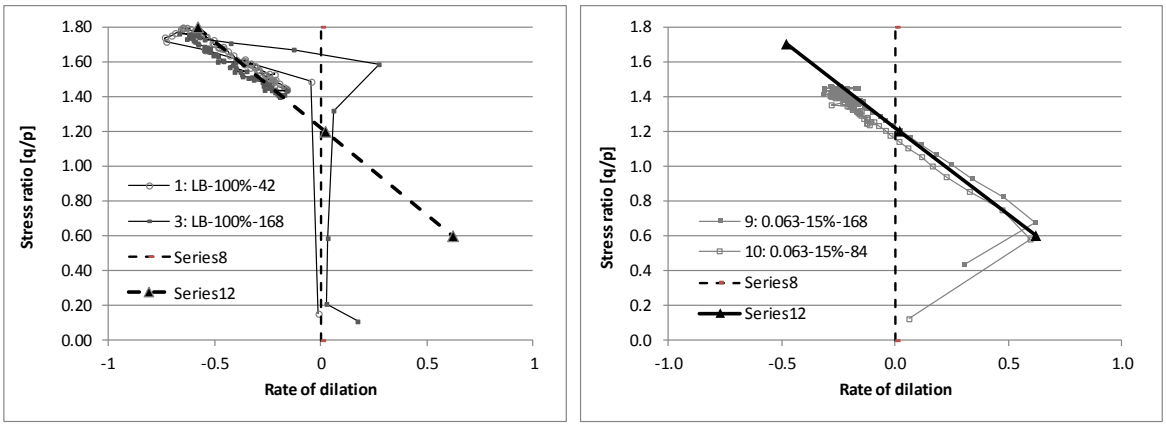

Fig. 14a. Stress-dilatancy for sand-only tests.
Fig. 14b. Stress-dilatancy for 0.063 mm DSS mixtures.

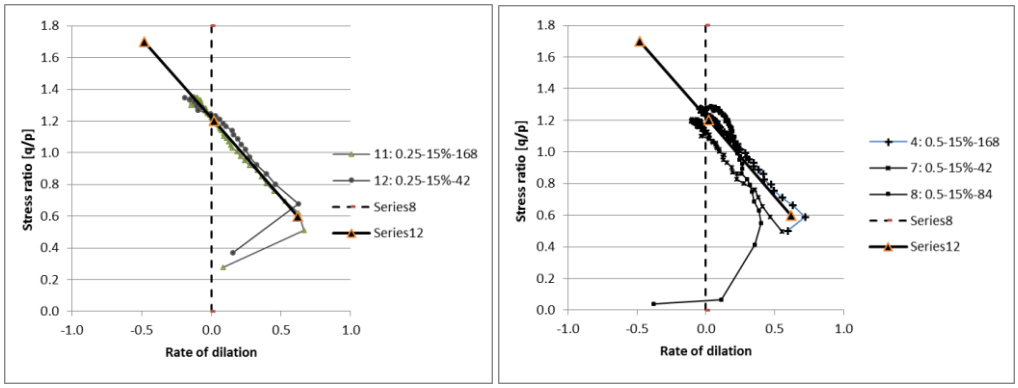

Fig. 14c. Stress-dilatancy for 0.25 mm dissolved salt-sand mixtures
Fig. 14d. Stress-dilatancy for 0.5 mm dissolved salt-sand mixtures.

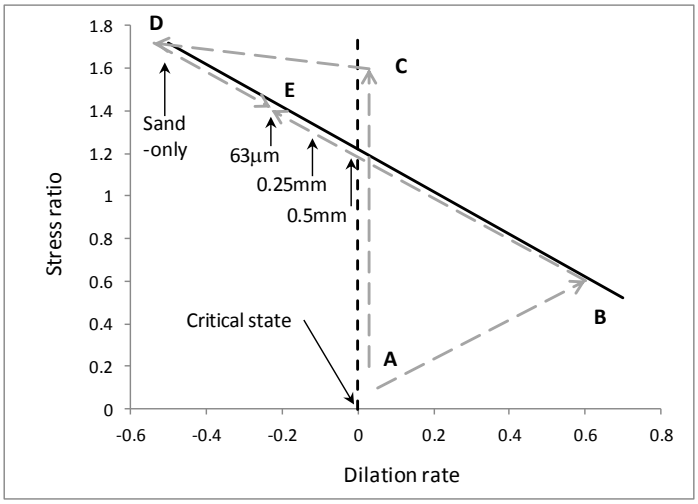

Fig. 15. Schematic figure of stress-dilatancy relationship, approach to stress-dilatancy relationship of sand-only (path ACDE), dissolved-salt-sand mixtures (path ABE), and maximum dilation rates and peak stress ratio for sand-only test and different dissolved-salt-sand mixtures.

Table 1. Test schedule showing salt fraction sizes, test condition, i.e. whether salt particles were intact or dissolved, and cell pressures under which tests were performed.

Test No	Salt particle size (mm)	Conditions	Cell pressure (kPa)	Test No	Salt particle size (mm)	Conditions	Cell pressure (kPa)
1	Sand only	Wet	42	4	0.5	Dissolved	168
3	Sand only	Wet	168	7	0.5	Dissolved	42
				8	0.5	Dissolved	84
22	0.5	Dry, intact	168	9	0.063	Dissolved	168
23	0.25	Dry, intact	168	10	0.063	Dissolved	84
25	0.063	Dry, intact	168	11	0.25	Dissolved	168
				12	0.25	Dissolved	42

Table 2. Typical volumes and volumetric states before and after dissolution of the salt fraction from a sample with overall dimensions: 50 mm diameter by 100 mm height. All volumes in ml and based on initial conditions and specific gravities given elsewhere in this section.

	Pre-dissolution	Post-dissolution (GDS = 15 ml)	Post-dissolution (GDS = 15.9 ml, i.e. +6%)
Total volume	196.35	181.35	180.45
Void volume	69.67	77.22	76.32
Salt volume (15% mass)	22.55	0	0
Sand volume (85% mass)	104.13	104.13	104.13
Specific volume	1.55	1.742	1.733

Table 3: Initial specific volumes, peak/maximum dilation rates and stress ratios for sand-only and salt-sand (intact and dissolved) mixture tests. M values for a Nova (1982) type stress dilatancy relationship with M values as stated and N = 0.2.

Test	Mixture, salt particle size	Post-dissolution specific volume	Dilation rate, at peak	Stress ratio, at peak	Steady state
Sand-only			D	η	$\eta = M$
3	-	1.54	-0.6	1.75	1.24
Salt intact					
25	0.063	1.44	-0.66	1.98	1.47
23	0.25	1.54	-0.50	1.77	1.38
22	0.5	1.56	-0.4	1.65	1.32
Salt dissolved					
9	0.063	1.67	-0.25	1.45	1.24
11	0.25	1.75	-0.13	1.35	1.24
4	0.5	1.77	no peak	no peak	1.24

Table 4: Initial specific volumes, peak/maximum dilation rates and stress ratios for sand-only and post dissolution mixture tests. M values for a Nova (1982) type stress dilatancy relationship with M values as stated and N = 0.2.

Test	Mixture, salt particle size [mm]	Pre-dissolution specific volume	Post dissolution specific volume	Dilation rate at peak/max	Stress ratio at peak/max	Critical state
Sand-only				D_{peak}	η_{peak}	$\eta = M$
1	-	1.53	-	-0.70	1.79	
3	-	1.54	-	-0.66	1.76	1.24
Salt dissolved						
9	0.063	1.38	1.67	-0.25	1.45	1.24
11	0.25	1.58	1.75	-0.13	1.35	1.24
4	0.5	1.60	1.77	-0.03 (max)	1.27 (max)	1.24
10	0.063	1.41	1.69	-0.28	1.42	1.24
12	0.25	1.55	1.75	-0.12	1.42	1.24
7	0.5	1.57	1.76	-0.06 (max)	1.20 (max)	1.24
8	0.5	1.58	1.76	0.05 (max)	1.28 (max)	1.24

Table 5: Average dilation rates and stress ratios for sand-only and each salt particle size tests, peak/maximum values.

Tests	Mixture, salt particle size [mm]	Initial[1] specific volume (average)	Dilation rate (average) at peak/max	Stress ratio (average) at peak/max	Critical state
			D_{peak}	η_{peak}	$\eta = M$
1, 3	Sand-only	1.53	−0.63	1.78	1.24
9, 10	0.063	1.68	−0.26	1.44	1.24
11, 12	0.25	1.75	−0.13	1.39	1.24
4, 7, 8	0.5	1.76	-0.01 (max)	1.25 (max)	1.24

[1] Refers to post-dissolution/pre-shearing in case of mixtures